Journal of Positive Sciences (JPS) **eISSN: 2582-9351, https://positive-sciences.com** **JPS. 2024 Jan; 5(1): 9-21**

Article info **Research Article**
Received on: 04.01.2025
Accepted on: 11.01.2025
Published on: 31.01.2025
doi: https://doi.org/10.52688/ASP85803

Sol-Gel Synthesis Reveals ZnO Nanoparticle Structure and Antibacterial Properties

Aseel S. Jasim [1 *]

[1] Biomass Energy Department, Al-Nahrain Renewable Energy Research Center, Al-Nahrain University, Jadriya, Baghdad, Iraq

[*] aseelsubhi11@nahrainuniv.edu.iq

ABSTRACT

The sol-gel technique was used to produce zinc oxide nanoparticles (ZnO NPs) from zinc nitrate in distilled water. With an average particle size of 21 nm, ZnO NPs form a wurtzite hexagonal shape. Four hours of 500°C heat purified nanopowder and decreased preparation pollutants. Structure and morphology were characterized by XRD, SEM, and EDS. Nanoparticle studies revealed crystalline structure and homogenous dispersion.

ZnO nanoparticles were examined for antibacterial activity against Gram-negative (Escherichia coli, Pseudomonas aeruginosa, and Klebsiella pneumoniae) and Gram-positive (Staphylococcus aureus) pathogens using conventional agar diffusion. Large zones of inhibition showed ZnO NPs' antibacterial capabilities. ZnO NPs disrupt bacterial cell membranes with ROS, making them antibacterial. This shows that calcination temperature and precursor selection improve ZnO nanoparticle shape and antibacterial activity. The findings suggest sol-gel-synthesized ZnO NPs might be employed in antibacterial coatings and water purification systems. Research on doping and functional modifications may increase multifunctional ZnO nanoparticle performance.

Keywords: XRD, FTIR, SEM-EDX, antibacterial activity, ZnO-NPs

INTRODUCTION

Zinc oxide (ZnO) has been a scientifically and technologically essential substance for a decade due to its flexibility and wide range of applications [1, 2]. ZnO is semiconducting, pyroelectric, piezoelectric, optoelectronic, and catalytic [3–5]. It is suitable for biosensors, light-emitting diodes, field-effect transistors, spintronic ferromagnetic materials, solar cells, photocatalysis, antibacterial compounds, and antioxidants [6–13]. The wide bandgap of 3.37 eV and high exciton binding energy of 60 meV make ZnO useful in many applications [14].

Nanoscale ZnO is popular because it performs better than bulk ZnO [15]. ZnO nanoparticles (NPs) are perfect for rubber manufacture, electrophotography, photoprinting, capacitors, protective coatings, antimicrobial agents, and conductive thin films for LCDs and blue laser diodes owing to their increased features [16] ZnO NPs' antimicrobial and antioxidant properties benefit medicine, cosmetics, and food [17]. ZnO nanoparticles fight several bacterial and fungal infections, making them beneficial in agriculture, food safety, and the environment [18].

*Corresponding author
Aseel S. Jasim,
Biomass Energy Department, Al-Nahrain Renewable Energy Research Center, Al-Nahrain University, Jadriya, Baghdad, Iraq
e-mail: aseelsubhi11@nahrainuniv.edu.iq

ZnO nanoparticles are made using sol-gel, anodization, co-precipitation, ultrasound-assisted, CVD, and mechanochemical-thermal synthesis [19]. Sol-gel nanoparticles have smaller diameters, larger specific surface areas, and greater purity than other approaches, making them appealing. High-quality ZnO nanoparticle production uses this method to manage phase composition, shape, and thermal stability [20].

Researchers have refined ZnO nanoparticle manufacturing parameters in recent years to increase their performance in many applications [21]. In particular, sol-gel creates ZnO nanoparticles with suitable structural and functional properties. Zinc nitrate and zinc acetate hydrolyze and condense with solvents and stabilizing agents. ZnO nanoparticles crystallize from gel after thermal treatment eliminates organic impurities [22].

XRD, SEM, and EDS examine ZnO nanoparticle phase composition, purity, thermal stability, and surface form. XRD shows crystalline structure and average grain size, whereas SEM and EDS provide nanoparticle form and elemental composition. Sol-gel zinc oxide nanoparticles show potential in photocatalysis, optoelectronics, and biomedicine. They destroy Gram-positive and Gram-negative bacteria, according to extensive research. ZnO nanoparticles are an interesting antibacterial option, especially as resistance grows.

Rapid antibiotic-resistant bacteria proliferation threatens global health, increasing mortality and healthcare costs. New antibiotics are needed to treat Staphylococcus aureus, Klebsiella pneumoniae, and Escherichia coli, which are becoming resistant. Zinc oxide nanoparticles (ZnO NPs) may be effective antimicrobials due to their wide bandgap, high binding energy, and ROS production. Synthesis optimization for purity, homogeneous particle size, and antibacterial action is challenging. Lack of understanding of how synthesis parameters like calcination temperature and precursor selection impact ZnO NPs' antibacterial activity restricts their usage in medicine and industry. To treat antibiotic-resistant bacteria using ZnO NPs, several concerns must be solved.

This study uses sol-gel to generate high-purity zinc oxide nanoparticles (ZnO NPs) and examine their structural, optical, and antibacterial properties. To optimize synthesis, the study alternates calcination temperatures for uniform particle size, thermal stability, and high crystallinity. To study nanoparticle structure and morphology, XRD, SEM, and EDS will be employed. ZnO NPs will be evaluated against Staphylococcus aureus, Klebsiella pneumoniae, and E. coli. This study will evaluate the best synthesis parameters and antibacterial efficacy of ZnO NPs as an alternative antibiotic for medical, agricultural, and environmental uses.

This study produced zinc oxide (ZnO) nanoparticles using the sol-gel method, which is recognized for its cleanliness, homogeneity, and controllability. Calcination temperature influenced ZnO nanoparticle structure, morphology, and antibacterial properties. XRD, SEM, and EDS characterized the nanoparticles' phase composition, crystallite size, and surface form. Antibacterial efficiency of ZnO nanoparticles against Gram-positive and Gram-negative pathogens such as Staphylococcus aureus, Klebsiella pneumoniae, and E. coli was also investigated. This study reveals that ZnO nanoparticle antibacterial efficacy depends on synthesis circumstances. The findings enhance ZnO's medicinal, agricultural, and environmental benefits and provide potential antimicrobial resistance therapies.

EXPERIMENTAL WORK

Sol-gel synthesis of zinc oxide nanoparticles (ZnO NPs) began with zinc nitrate. To establish homogeneity, 11.6303 g zinc nitrate was dissolved in 100 ml distilled water and agitated at 70°C for three hours. The precursor solution was calcined at 300°C, 400°C, and 500°C for four hours. Each temperature setting produced 5 g of ZnO nanopowder from calcined samples. As shown in Fig. 1, 500°C calcination removed organic residues and impurities, creating a pure crystalline phase.

*Corresponding author
Aseel S. Jasim,
Biomass Energy Department, Al-Nahrain Renewable Energy Research Center, Al-Nahrain University, Jadriya, Baghdad, Iraq
e-mail: aseelsubhi11@nahrainuniv.edu.iq

XRD, SEM, and EDS were used to characterize ZnO nanoparticles' structural and morphological features. ZnO's wurtzite hexagonal structure with a 21 nm average crystallite size was found by XRD. SEM pictures revealed homogenous nanoparticles, whereas EDS validated elemental composition.

ZnO NPs were tested for Gram-negative (Escherichia coli, Pseudomonas aeruginosa, and Klebsiella pneumoniae) and Gram-positive (Staphylococcus aureus) antibacterial activity using agar well diffusion. Nanoparticles showed significant inhibitory zones, indicating their antibacterial activity. ZnO NPs may be used in biomedical and environmental domains due to their ability to generate reactive oxygen species (ROS) and break bacterial cell membranes.

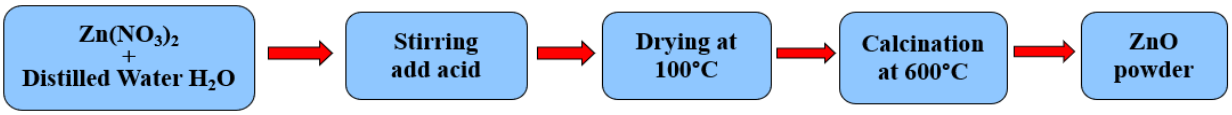

Fig. 1. Sol gel ZnO-NPs production schematic

RESULTS AND DISCUSSION

XRD

XRD confirmed the hexagonal wurtzite structure of ZnO nanoparticles, similar to JCPDS card 36-1451. Significant diffraction peaks at 2θ values of 32.21°, 34.632°, 36.121°, 48.334°, and 57.446° correspond to the crystallographic planes (100), (002), (101), (102), and (110) [23]. Sharp peaks imply high crystallinity of produced ZnO nanoparticles. To assess physical characteristics, crystallite size, lattice parameters, unit cell volume, microstrain, and dislocation density were computed.

Scherrer's equation computed crystallite size (D) [24]:

$$D = \frac{K\lambda}{\beta\cos\theta} \quad (1)$$

where K = shape factor (0.9), λ = X-ray wavelength (1.5406 Å), β = FWHM in radians, and θ = Bragg angle. The ZnO sample showed a computed average crystallite size of 28.91 nm, indicating its nanoscale nature. The tiny crystallite size increases surface area, which is important for photocatalysis and antibacterial action.

For a hexagonal system, Bragg's rule and the following equation determined lattice parameters a, b, and c [25].

$$\frac{1}{d^2} = \frac{4}{3}\left(\frac{h^2+hk+k^2}{a^2}\right) + \frac{l^2}{c^2} \quad (2)$$

where h, k, and l are Miller indices and d is interplanar spacing. The estimated lattice parameters were a=b=3.249 Å and c=2.885 Å. These results match ZnO standard values, confirming the hexagonal wurtzite phase synthesis without lattice distortion.

Unit cell volume (V) was estimated using the hexagonal structure formula [26].

$$V = \frac{\sqrt{3}}{2}a^2c \quad (3)$$

The calculated unit cell capacity was 47.83 $A^{\circ 3}$. This number matches ZnO nanoparticle volume, verifying the produced material's dependability.

*Corresponding author
Aseel S. Jasim,
Biomass Energy Department, Al-Nahrain Renewable Energy Research Center, Al-Nahrain University, Jadriya, Baghdad, Iraq
e-mail: aseelsubhi11@nahrainuniv.edu.iq

To compute microstrain (ε), which represents lattice distortions, use the relation [27].

$$\varepsilon = \frac{\beta}{4\tan\theta} \quad (4)$$

The average microstrain for ZnO nanoparticles was 1.20×10^{-3}. Low microstrain indicates minimum lattice distortions, which helps nanoparticle structural stability. A defect density metric, dislocation density (δ), was calculated using the equation [28].

$$\delta = \frac{1}{D^2} \quad (5)$$

The estimated dislocation density was 1.54×10^{-3} nm^{-2}. This low number indicates the nanoparticles' strong crystallinity, which is necessary for optoelectronics and antibacterial treatments.

The structural study shows that ZnO nanoparticles have good crystallinity, nanoscale size, and few flaws, making them appropriate for many applications. The high crystallinity optimizes optoelectronic device performance, while the tiny crystallite size and large surface area facilitate bacterial cell contact and antimicrobial activity. These results demonstrate ZnO nanoparticles' adaptability and usefulness as multifunctional nanotechnology materials [29].

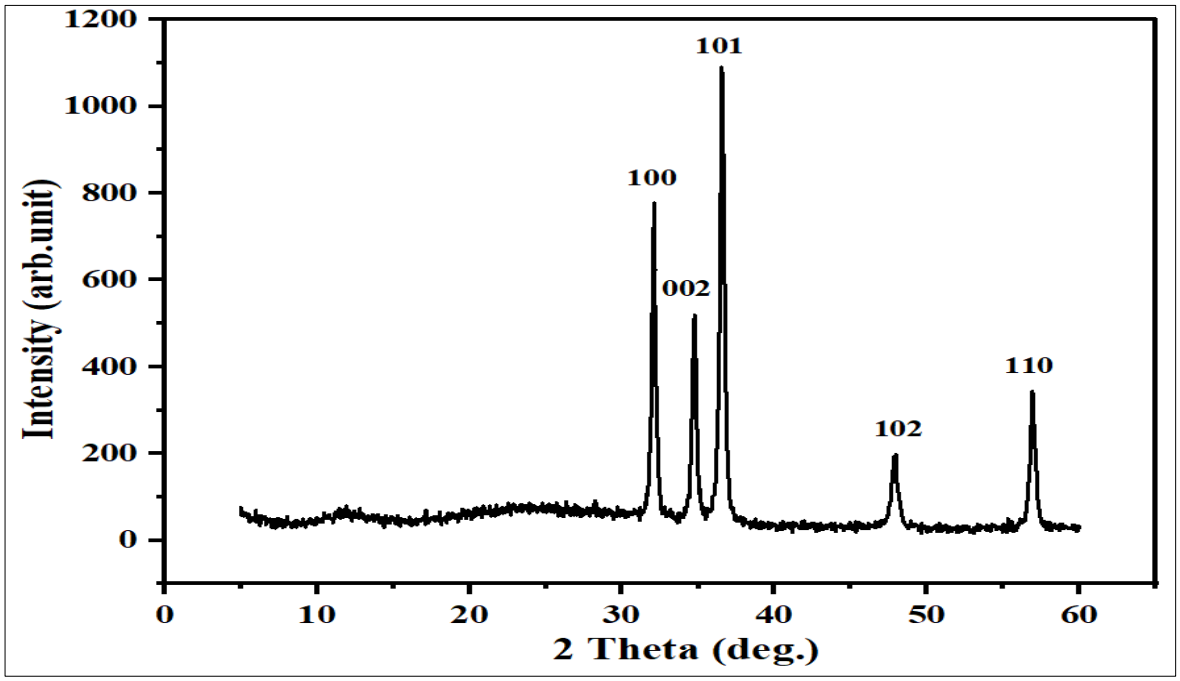

Fig. 2. Sol gel-synthesized ZnO-NPs XRD pattern

*Corresponding author
Aseel S. Jasim,
Biomass Energy Department, Al-Nahrain Renewable Energy Research Center, Al-Nahrain University, Jadriya, Baghdad, Iraq
e-mail: aseelsubhi11@nahrainuniv.edu.iq

Table 1. XRD parameters of ZnO-NPs synthesis by the sol gel method

Sample	2θ (o)	(hkl)	β (o)	d-Spacing (A)	D_{ave} (nm)	V ($Å^3$)	Micro strain (ε)	Dislocation density (δ) $(nm)^{-2}$
ZnO	32.21	(100)	0.3782	2.776	218.64	47.83	1.35×10^{-3}	1.87×10^{-3}
	34.632	(002)	0.4135	2.589	201.24		1.48×10^{-3}	2.21×10^{-3}
	36.121	(101)	0.4128	2.482	202.42		1.47×10^{-3}	2.20×10^{-3}
	48.334	(102)	0.2342	1.881	371.80		0.83×10^{-3}	0.69×10^{-3}
	57.446	(110)	0.2444	1.604	370.66		0.87×10^{-3}	0.74×10^{-3}
Average					212.35		1.20×10^{-3}	1.54×10^{-3}

The Williamson-Hall method is represented by the equation [30]:

$$\beta \cdot \cos(\theta) = \frac{K \cdot \lambda}{D} + 4 \cdot \varepsilon \cdot \sin(\theta) \quad (6)$$

where β is the broadening of the peak, D is the crystallite size, ε is the microstrain, λ is the wavelength, and θ is the Bragg angle.

ZnO nanoparticle crystallite size was determined using the Scherrer equation and the Williamson-Hall (W-H) technique. The Scherrer equation gives an average crystallite size of 212.35 nm. This is a typical nanoparticle X-ray diffraction peak broadening estimate. The Williamson-Hall technique yielded a -318.81 nm crystallite size using a linear regression of β×cos(θ) vs. 4×sin(θ) with a slope of -0.00435. However, the negative value signals data issues, either owing to experimental or instrumental variables like excessive instrumental broadening or non-ideal data behavior. In circumstances with atypical data behavior, the Williamson-Hall approach is limited. Since the W-H approach did not provide physically significant findings, the Scherrer equation gives a more accurate crystallite size estimate in this investigation.

FTIR

The sol-gel-synthesized ZnO nanoparticles' FTIR spectrum reveals the material's functional groups and chemical bonds, which affect its structural and antibacterial capabilities. O-H stretching vibrations of hydroxyl groups provide a large peak at 3448.72 cm^{-1}, suggesting surface-adsorbed water or leftover hydroxyl groups from synthesis. ZnO nanoparticles' surface reactivity depends on these hydroxyl groups, which generate reactive oxygen species (ROS) that boost antibacterial activity. Peaks at 2924.09 cm^{-1} and 2852.72 cm^{-1} indicate asymmetric and symmetric C-H bond stretching vibrations, indicating organic residues from sol-gel precursors. This suggests insufficient organic material removal during calcination, which might be enhanced in future research [31].

The peak at 2360.87 cm^{-1} is attributed to the vibrational modes of CO_2 molecules adsorbing on the nanoparticle surface, a frequent phenomenon owing to ambient CO_2 interaction. The signal at 1741.72 cm^{-1} is believed to be the stretching vibration of carbonyl (C=O) groups from leftover chemical intermediates during the sol-gel synthesis. The signal at 1627.93 cm^{-1}, ascribed to O-H bending vibrations, confirms water molecule adsorption on ZnO nanoparticles.

This surface water helps nanoparticles interact with microorganisms. An further signal at 1458.18 cm^{-1}, linked to C-H bending vibrations, confirms organic remains. Lastly, the peak at 875.68 cm^{-1} reflects Zn-O stretching vibrations, a unique ZnO structural fingerprint. This proves crystalline ZnO nanoparticles were formed. These functional groups indicate that nanoparticles have a highly reactive surface, making them antimicrobial. Optimizing the calcination procedure might minimize organic residues and increase nanoparticle purity, increasing their performance in diverse applications (Fig. 3 and Table 2).

*Corresponding author
Aseel S. Jasim,
Biomass Energy Department, Al-Nahrain Renewable Energy Research Center, Al-Nahrain University, Jadriya, Baghdad, Iraq
e-mail: aseelsubhi11@nahrainuniv.edu.iq

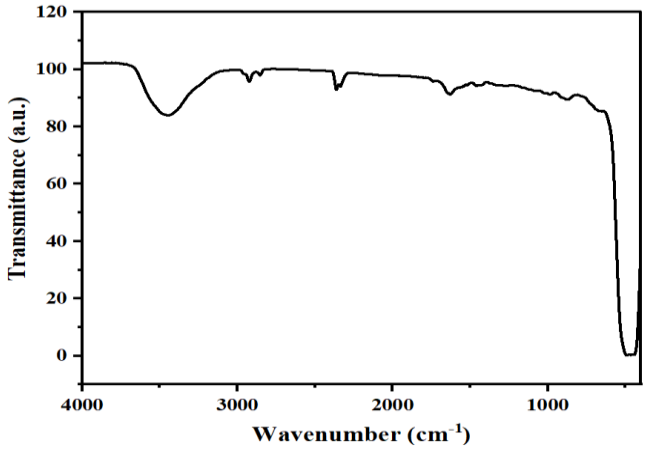

Fig. 3. The sol-gel technique produces ZnO NPs with an FTIR spectrum

Table 2. Sol-gel-synthesized ZnO nanoparticle FTIR data

Wavenumber (cm^{-1})	Functional Group/Mode	Assignment	Interpretation
3448.72	O-H Stretching	Hydroxyl groups (adsorbed water or residual hydroxyls)	Indicates surface reactivity and potential for ROS generation, enhancing antibacterial activity.
2924.09	C-H Asymmetric Stretching	Organic residues from precursors	Suggests incomplete removal of organic material during calcination.
2852.72	C-H Symmetric Stretching	Organic residues from precursors	Confirms presence of organic material, indicating optimization in synthesis is required.
2360.87	CO_2 Adsorption	Vibrations of adsorbed carbon dioxide molecules	Represents interaction of ZnO nanoparticles with atmospheric CO_2.
1741.72	C=O Stretching	Carbonyl group vibrations	Likely due to residual organic intermediates from the sol-gel process.
1627.93	O-H Bending	Adsorbed water molecules	Confirms the presence of surface water, enhancing interaction with bacterial cells.
1458.18	C-H Bending	Organic residue vibrations	Suggests the presence of carbon-based compounds, linked to incomplete calcination.
875.68	Zn-O Stretching	Vibrations of Zn-O bond	Confirms the successful formation of ZnO nanoparticles with characteristic crystalline structure.

*Corresponding author
Aseel S. Jasim,
Biomass Energy Department, Al-Nahrain Renewable Energy Research Center, Al-Nahrain University, Jadriya, Baghdad, Iraq
e-mail: aseelsubhi11@nahrainuniv.edu.iq

UV CURVE

As illustrated in Fig. 4, ZnO nanopowder's 350 nm absorption peak is its bandgap, demonstrating semiconductivity. Zinc oxide (ZnO) has a broad bandgap of 3.37 eV, as seen by this absorption peak energy [32]. The material's 350 nm absorption peak indicates significant UV absorption, typical of ZnO. Electrons moving from the valence band to the conduction band need energy greater than the bandgap, causing this absorption. Due to its UV absorption peak, ZnO nanoparticles are promising for optoelectronics and UV-based devices.

The computed energy gap (Eg) of 3.37 eV for ZnO matches bulk ZnO characteristics. Particle size and synthesis procedure affect ZnO's optical properties, narrowing or widening the bandgap. The energy gap of 3.37 eV suggests well-formed ZnO nanoparticles that retain their optical properties, which are necessary for photocatalytic and antibacterial activities. ZnO's bandgap implies it might be employed for photocatalysis, such as breaking down organic pollutants under UV light and emitting and detecting UV light. Nanoparticle electrical properties and stability are affected by the energy gap, making them valuable in sensors, solar cells, and photocatalytic devices.

In ZnO nanopowder, the absorption peak is 350 nm. Value substitution:

$$\mathrm{Eg} = \frac{(6.626 \times 10 - 34\,\mathrm{J\backslash s})(3.0 \times 108\,\mathrm{m/s})}{350 \times 10 - 9\,\mathrm{m}}$$

Simplifying the equation:

$$\mathrm{Eg} = \frac{(1.9878 \times 10 - 25)}{350 \times 10 - 9}\mathrm{J} = 5.68 \times 10^{-19}\mathrm{J}$$

To convert joules to electron volts (eV), we use the relation: $1\,\mathrm{eV} = 1.602 \times 10^{-19}\,\mathrm{J}$

So:

$$\mathrm{Eg} = \frac{5.68 \times 10^{-19}}{1.602 \times 10^{-19}}\,\mathrm{eV} \approx 3.37\,\mathrm{eV}$$

To determine photon energy E in electron volts (eV) from wavelength λ, use the following equation:

$$\mathrm{E} = \frac{1240}{\lambda} \tag{6}$$

The equation uses λ (nm) as the wavelength and 1240 as the constant calculated from Planck's constant and light speed. This equation calculates photon energy based on wavelength, which helps explain the material's optical absorption.

Next, calculate the absorption coefficient α using the method [33]:

$$\alpha = \frac{2.303 \times \mathrm{A}}{\mathrm{d}} \tag{7}$$

where A is material absorbance and d is sample thickness, usually 1 cm. The absorption coefficient shows how much light the material absorbs at a particular wavelength by relating its optical qualities to photon energy.

Final analysis uses the Tauc relation to determine the material's optical bandgap. Equation follows [34]:

$$(\alpha h\nu)^{n} = \mathrm{B}(h\nu - \mathrm{Eg}) \tag{8}$$

*Corresponding author
Aseel S. Jasim,
Biomass Energy Department, Al-Nahrain Renewable Energy Research Center, Al-Nahrain University, Jadriya, Baghdad, Iraq
e-mail: aseelsubhi11@nahrainuniv.edu.iq

For this equation, α represents absorption coefficient, hv represents photon energy, Eg represents optical bandgap, and B is a constant. Electronic transition exponents vary (n=1/2 for direct and n=2 for indirect). Plotting (αhv)n against hv reveals the optical bandgap Eg from the x-intercept of the linear area (refer to Fig. 4 inset).

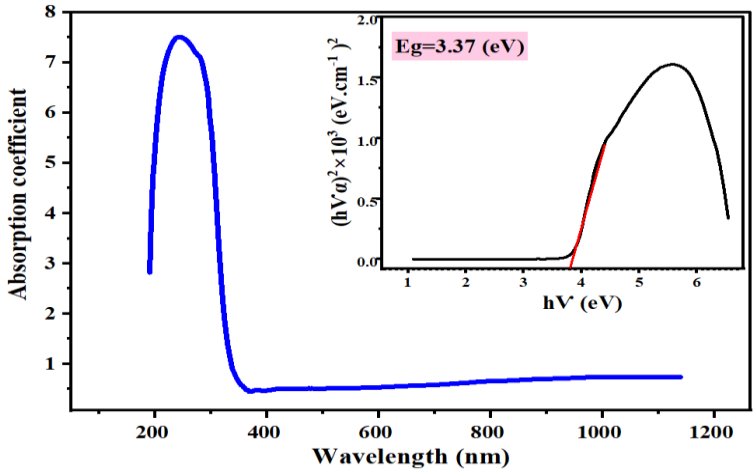

Fig. 4. Absorptance and Energy Gap of ZnO Nanopowder

The absorption peak at 350 nm corresponds to the energy required for electrons in the valence band of ZnO to be excited to the conduction band. This energy is equal to the energy gap of the material, and for ZnO, it is found to be 3.37 eV, which falls within the UV range. This energy gap is characteristic of semiconductors, particularly those with wide bandgaps such as ZnO.

The energy gap of ZnO nanoparticles can sometimes be larger than the bulk material due to quantum confinement effects. These effects arise because the smaller size of nanoparticles leads to a higher density of states and affects the electronic properties, including the bandgap. However, in this case, the value of 3.37 eV is consistent with the bulk ZnO material, indicating that the nanoparticles retain the expected optical properties.

The wide bandgap of 3.37 eV enables ZnO nanoparticles to absorb UV light efficiently, making them useful for photocatalytic applications, including the degradation of organic pollutants and antibacterial applications under UV exposure. The ability to absorb UV light and catalyze reactions is a key feature for applications in environmental sustainability and clean energy.

ENERGY DISPERSIVE X-RAY SPECTROSCOPY (EDX)

The sol-gel-synthesized ZnO nanoparticles (ZnO-NPs) Energy Dispersive X-ray (EDX) analysis findings are shown in Fig. 5 and Table 3. As predicted for ZnO nanoparticles, zinc (Zn) dominates at 84.10% by weight. ZnO, which contains oxygen, is confirmed by 15.58% by weight of oxygen (O). Ca is also discovered at 0.32%, which may suggest contamination or calcium impurities in the synthesis process. Sigma values show the standard deviations of weight percentages, showing measurement accuracy. These findings validate the high-purity production of ZnO nanoparticles, whereas the little amount of calcium does not change the composition.

*Corresponding author
Aseel S. Jasim,
Biomass Energy Department, Al-Nahrain Renewable Energy Research Center, Al-Nahrain University, Jadriya, Baghdad, Iraq
e-mail: aseelsubhi11@nahrainuniv.edu.iq

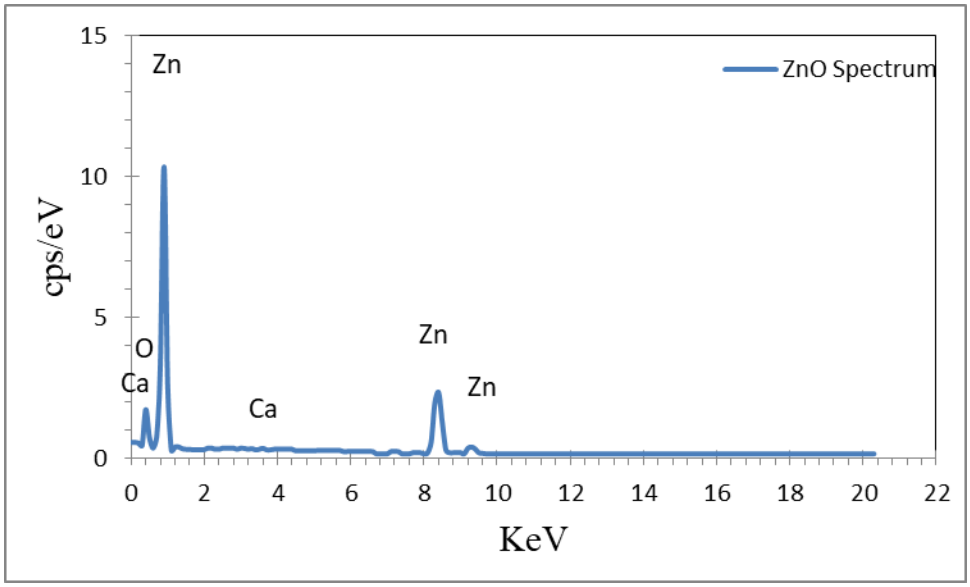

Fig. 5. ZnO nanopowder absorption and energy gap

Table 3. Sol gel-synthesized ZnO-NPs EDX values

Element	Wt.%	Wt.% Sigma
O	15.58	0.26
Ca	0.32	0.07
Zn	84.10	0.27
Total:	100.00	

SEM AND EDS ANALYSIS

Since the form and size of ZnO nanoparticles (ZnO-NPs) considerably impact their ability to prevent bacterial growth, many studies have examined their antibacterial capabilities [6]. The morphology of ZnO-NPs is highly dependent on the conditions during their synthesis, and researchers have reported various shapes such as nanorods, nanowires, nanotubes, nanospheres, nanoneedles, drums, nanorings, spirals, polyhedrons, flowers, discs, plates, stars, and boxes [7, 8]. Each of these shapes exhibits distinct physicochemical properties, which can be attributed to the specific synthesis methods used to create them. The synthesis mechanisms involve several key factors, including the choice of precursor materials, solvent type, pH levels, and temperature, all of which can influence the final morphology of the nanoparticles.

In this study, the ZnO-NPs were synthesized under controlled conditions, resulting in the formation of a hexagonal wurtzite structure, as shown in Fig. 6 (a). The hexagonal shape is well-known for its stability and high surface area, which contribute to the enhanced antibacterial activity of ZnO nanoparticles. Fig. 6 (b) shows that the average particle size was 51.31 nm, which is ideal for antibacterial applications. Smaller nanoparticles have more surface area, which helps them damage bacterial membranes. ZnO-NPs are interesting biomedical and environmental materials because they may be shaped to enhance antibacterial effectiveness by adjusting synthesis parameters.

*Corresponding author
Aseel S. Jasim,
Biomass Energy Department, Al-Nahrain Renewable Energy Research Center, Al-Nahrain University, Jadriya, Baghdad, Iraq
e-mail: aseelsubhi11@nahrainuniv.edu.iq

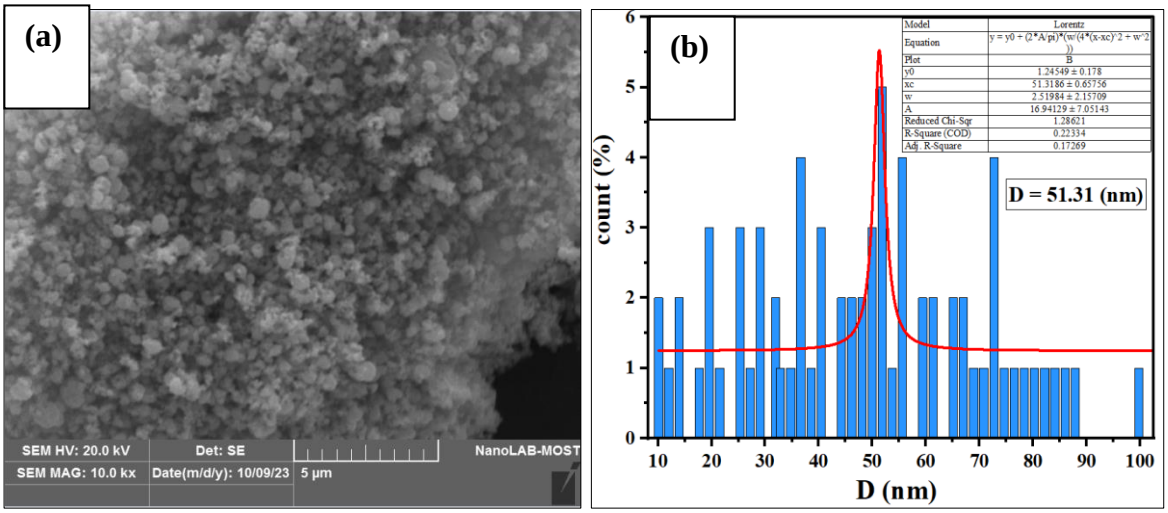

Fig. 6. (a) SEM picture of sol-gel-synthesized ZnO nanoparticles and (b) particle size distribution

MECHANISM OF BACTERIA

ZnO nanoparticles (NPs) were tested for their antibacterial effects on Gram-negative and Gram-positive bacteria cell division. Polymerization of the FtsZ protein creates the division septum and aids bacterial cell wall production. Bacterial division pathways are disrupted by ZnO NPs, reducing cell growth and proliferation. Nanoparticles affect protein synthesis, cell division, and cell wall integrity, killing bacteria [35].

ZnO NPs were tested for antibacterial activity against Escherichia coli, Pseudomonas aeruginosa, Klebsiella pneumoniae, and Staphylococcus aureus on Mueller-Hinton agar medium using the zone of inhibition (ZOI) technique. Fig. 7 and Table 4 reveal that ZnO NPs inhibit all bacterial strains to various degrees. E. coli had the biggest inhibitory zone (28 mm), followed by Klebsiella pneumoniae (24 mm) and Staphylococcus aureus (21 mm). With a 6 mm inhibitory zone, ZnO nanoparticles had no effect on Pseudomonas aeruginosa.

ZnO NPs create ROS when they come into contact with bacterial cells, which is why they are antibacterial. ROS cause oxidative stress, which damages bacterial membranes, breaks DNA, and kills cells. ZnO NPs also break bacterial cell walls, boosting their antibacterial action. These results demonstrate ZnO nanoparticles' antibacterial potential for medicinal and infection control applications. Antibacterial activity may vary by strain due to bacterial cell wall composition and nanoparticle resistance. Nanomaterial efficiency for antibacterial applications depends on understanding strain-specific responses [36].

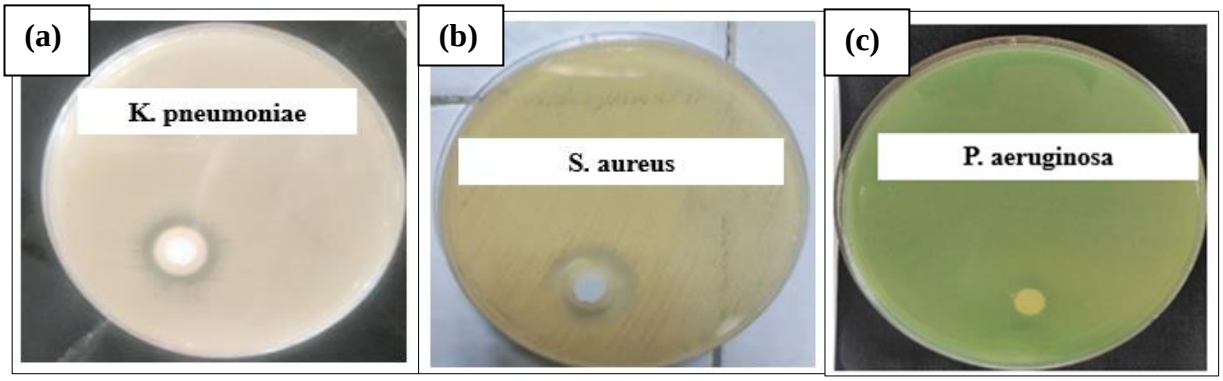

Fig. 7. ZnO nanoparticle action on K. pneumoniae, S. aureus, and P. aeruginosa

*Corresponding author
Aseel S. Jasim,
Biomass Energy Department, Al-Nahrain Renewable Energy Research Center, Al-Nahrain University, Jadriya, Baghdad, Iraq
e-mail: aseelsubhi11@nahrainuniv.edu.iq

Table 4. ZnO nanopowder bacteria activity

Sample	Klebsiella	S. Aureus	E. coli	Pseudomonas aeruginosa
ZnO	24 mm	21 mm	28 mm	6 mm

CONCLUSION

Sol-gel-synthesized ZnO nanoparticles (NPs) are analyzed for structural, optical, and antibacterial characteristics. XRD examination showed a hexagonal wurtzite structure with a 51.31 nm crystalline size, a ZnO hallmark. This structural consistency was corroborated by Fourier Transform Infrared (FTIR) spectroscopy, which detected Zn–O bonds and verified nanoparticle purity.

ZnO's direct band gap of 3.37 eV, measured by UV-Vis absorption spectroscopy, suggests optoelectronic possibilities. The UV absorption spectrum energy gap supports photocatalytic and antimicrobial applications. Energy Dispersive X-ray (EDX) examination verified that the produced nanoparticles were mostly zinc and oxygen with no contaminants.

SEM imaging showed consistent ZnO particle distribution and shape, which is necessary for their strong antibacterial activity. The zone of inhibition approach was used to assess ZnO nanoparticles' antibacterial efficacy against Gram-negative and Gram-positive bacteria. A 21-28 mm inhibitory zone demonstrated substantial antibacterial efficacy against Escherichia coli, Klebsiella pneumoniae, and Staphylococcus aureus. The nanoparticles had no effect on Pseudomonas aeruginosa, showing that bacterial strains had different antibacterial properties. ZnO nanoparticles have strain-specific antibacterial activity and great potential for optimization in antimicrobial and optoelectronic applications.

REFERENCES

[1] A. Singh, F. Wan, K. Yadav, S. Kharbanda, P. Thakur, and A. Thakur, “A novel magnetic NiFe2O4-Ag-ZnO hybrid nanocomposite for the escalated photocatalytic dye degradation and antibacterial activities,” Materials Science and Engineering B, vol. 299, p. 116935, Oct. 2023, doi: 10.1016/j.mseb.2023.116935.

[2] D. Debnath, D. Sen, T. T. Neog, B. Saha, and S. K. Ghosh, “Growth of ZNO polytypes: multiple facets of diverse applications,” Crystal Growth & Design, vol. 24, no. 3, pp. 871–885, Jan. 2024, doi: 10.1021/acs.cgd.3c01076.

[3] D. Wang et al., “Piezoelectric polarization induced by dual piezoelectric materials ZnO nanosheets/MoS2 heterostructure for enhancing photoelectrochemical water splitting,” Journal of Colloid and Interface Science, vol. 653, pp. 1166–1176, Sep. 2023, doi: 10.1016/j.jcis.2023.09.157.

[4] J. Wang et al., “Piezo-phototronic effect modulated optoelectronic artificial synapse based on a-Ga2O3/ZnO heterojunction,” Nano Energy, vol. 120, p. 109128, Nov. 2023, doi: 10.1016/j.nanoen.2023.109128.

[5] Y. Shen et al., “g-ZnO/Si9C15: a S-scheme heterojunction with high carrier mobility for photo-electro catalysis of water splitting,” Physical Chemistry Chemical Physics, vol. 26, no. 6, pp. 5569–5578, Jan. 2024, doi: 10.1039/d3cp04933g.

[6] B. Brasiunas, A. Popov, V. Lisyte, A. Kausaite-Minkstimiene, and A. Ramanaviciene, “ZnO nanostructures: A promising frontier in immunosensor development,” Biosensors and Bioelectronics, vol. 246, p. 115848, Nov. 2023, doi: 10.1016/j.bios.2023.115848.

[7] M. Ning et al., “Passivating defects in ZnO electron transport layer for enhancing performance of red InP-based quantum dot light-emitting diodes,” Materials Research Bulletin, vol. 170, p. 112589, Oct. 2023, doi: 10.1016/j.materresbull.2023.112589.

[8] H. Yuan, H. Shimotani, A. Tsukazaki, A. Ohtomo, M. Kawasaki, and Y. Iwasa, “High-Density carrier accumulation in ZNO Field-Effect transistors gated by electric double layers of ionic liquids,” Advanced Functional Materials, vol. 19, no. 7, pp. 1046–1053, Feb. 2009, doi: 10.1002/adfm.200801633.

[9] A. T. Naziba et al., “Structural, optical, and magnetic properties of Co-doped ZnO nanorods: Advancements in room temperature ferromagnetic behavior for spintronic applications,” Journal of Magnetism and Magnetic Materials, vol. 593, p. 171836, Feb. 2024, doi: 10.1016/j.jmmm.2024.171836.

*Corresponding author
Aseel S. Jasim,
Biomass Energy Department, Al-Nahrain Renewable Energy Research Center, Al-Nahrain University, Jadriya, Baghdad, Iraq
e-mail: aseelsubhi11@nahrainuniv.edu.iq

[10] S. Wang, S. Zhang, Z. Liu, J. Wang, J. Xu, and L. Yu, "High-performance radial junction solar cells on ZnO coated stainless steel with excellent flexibility and durability," Nano Energy, vol. 122, p. 109262, Jan. 2024, doi: 10.1016/j.nanoen.2024.109262.

[11] H. Yu, M. Zhao, C. Xue, J. Huang, N. Zhao, and L. Kong, "All-solid-state Z-scheme nanojunction PW12/Ag/ZnO photocatalyst: Effective carriers transfer promotion and enhanced visible light driven," Journal of Molecular Structure, vol. 1300, p. 137272, Dec. 2023, doi: 10.1016/j.molstruc.2023.137272.

[12] L. Zhang, Y. Ding, M. Povey, and D. York, "ZnO nanofluids – A potential antibacterial agent," Progress in Natural Science Materials International, vol. 18, no. 8, pp. 939–944, May 2008, doi: 10.1016/j.pnsc.2008.01.026.

[13] R. Sonkar, N. J. Mondal, B. Boro, M. P. Ghosh, and D. Chowdhury, "Cu doped ZnO nanoparticles: Correlations between tuneable optoelectronic, antioxidant and photocatalytic activities," Journal of Physics and Chemistry of Solids, vol. 185, p. 111715, Oct. 2023, doi: 10.1016/j.jpcs.2023.111715.

[14] H. Barkat, E. G. Temam, H. B. Temam, N. Mokrani, S. Rahmane, and M. Althamthami, "Enhancing Sunlight-Driven photocatalysis: high transparency and hydrophilic advancements in BA-Doped ZNO thin films," Journal of Materials Engineering and Performance, Sep. 2024, doi: 10.1007/s11665-024-10126-0.

[15] E. V. Hernández, C. E. C. Montufar, M. A. C. Ramírez, and F. M. Hernández, "Photoluminescence of Erbium-Doped ZNO nanostructures," Materials Science Forum, vol. 1112, pp. 139–144, Feb. 2024, doi: 10.4028/p-gw795b.

[16] Y. Hao et al., "Robust and Reliable Organic Dye-Embedded Zinc Oxide Nanocomposite Phosphor with a Broad Spectrum and High Efficiency Enables an Eco-Friendly White Laser Light Diode," ACS Sustainable Chemistry & Engineering, vol. 12, no. 17, pp. 6738–6747, Apr. 2024, doi: 10.1021/acssuschemeng.4c01014.

[17] M. J. Mohammadi, M. Hosseinzadeh, and S. Salmanpour, "The effect of flaxseed extract incorporated with nano ZnO and ZnO-Mg on the physicochemical, mechanical, and antioxidant properties of sago starch films," Journal of Food Measurement & Characterization, vol. 18, no. 8, pp. 6803–6815, Jun. 2024, doi: 10.1007/s11694-024-02694-5.

[18] M. Liaqat et al., "Investigate the effect of ZnO/Bi2O3 nanocomposite: A synergistic versatile approach for biomedical and environmental applications," Colloids and Surfaces a Physicochemical and Engineering Aspects, vol. 681, p. 132773, Nov. 2023, doi: 10.1016/j.colsurfa.2023.132773.

[19] S. Nazir et al., "Metal-based nanoparticles: basics, types, fabrications and their electronic applications," Zeitschrift Für Physikalische Chemie, vol. 238, no. 6, pp. 965–995, Jan. 2024, doi: 10.1515/zpch-2023-0375.

[20] P. Phogat, N. Shreya, R. Jha, and S. Singh, "Synthesis of novel ZnO nanoparticles with optimized band gap of 1.4 eV for high-sensitivity photo electrochemical detection," Materials Today Sustainability, vol. 27, p. 100823, May 2024, doi: 10.1016/j.mtsust.2024.100823.

[21] P. Phogat, N. Shreya, R. Jha, and S. Singh, "Harnessing ZnO morphologies in energy application and sustainable development," Physica Scripta, vol. 99, no. 10, p. 102004, Sep. 2024, doi: 10.1088/1402-4896/ad7990.

[22] C. Hu, F. Lu, J. Ma, and R. Zhiani, "Dendritic Filamentary Bi7O9I3 Modified with ZnO for Green Removal of Organic Dyes Compounds," Catalysis Letters, vol. 154, no. 7, pp. 3332–3345, Jan. 2024, doi: 10.1007/s10562-023-04559-w.

[23] H. Q. N. M. Al-Arique, S. S. S. Al-Qadasy, N. M. S. Kaawash, S. Q. Chishty, and K. A. Bogle, "Study the characterization of ZnO and AZO films prepared by spray pyrolysis and the effect of annealing temperature," Optical Materials, vol. 150, p. 115261, Mar. 2024, doi: 10.1016/j.optmat.2024.115261.

[24] N. J. Tamanna, Md. S. Hossain, N. M. Bahadur, and S. Ahmed, "Green synthesis of Ag2O & facile synthesis of ZnO and characterization using FTIR, bandgap energy & XRD (Scherrer equation, Williamson-Hall, size-train plot, Monshi- Scherrer model)," Results in Chemistry, vol. 7, p. 101313, Jan. 2024, doi: 10.1016/j.rechem.2024.101313.

[25] U. Javed, H. A. Sohail, A. Nazneen, M. Atif, G. M. Mustafa, and M. I. Khan, "Tuning of structural, magnetic, and optical properties of ZNO nanoparticles by Co and CU doping," Solid State Communications, vol. 390, p. 115616, Oct. 2024, doi: 10.1016/j.ssc.2024.115616.

[26] M. Anandan, S. Dinesh, B. Christopher, N. Krishnakumar, B. Krishnamurthy, and M. Ayyar, "Multifaceted investigations of co-precipitated Ni-doped ZnO nanoparticles: Systematic study on structural integrity, optical interplay and photocatalytic performances," Physica B Condensed Matter, vol. 674, p. 415597, Dec. 2023, doi: 10.1016/j.physb.2023.415597.

[27] A. S. Abdel-Rahman and Y. A. Sabry, "An approach to the micro-strain distribution inside nanoparticle structure," International Journal of Non-Linear Mechanics, vol. 161, p. 104670, Feb. 2024, doi: 10.1016/j.ijnonlinmec.2024.104670.

[28] V. Kaushik, K. Bhardwaj, D. Kumar, M. Kumar, and S. K. Sharma, "Effect of various processing parameters on the properties of ZnO thin films," Hybrid Advances, p. 100295, Sep. 2024, doi: 10.1016/j.hybadv.2024.100295.

[29] E. L. Irede et al., "Cutting-edge developments in zinc oxide nanoparticles: synthesis and applications for enhanced antimicrobial and UV protection in healthcare solutions," RSC Advances, vol. 14, no. 29, pp. 20992–21034, Jan. 2024, doi: 10.1039/d4ra02452d.

*Corresponding author
Aseel S. Jasim,
Biomass Energy Department, Al-Nahrain Renewable Energy Research Center, Al-Nahrain University, Jadriya, Baghdad, Iraq
e-mail: aseelsubhi11@nahrainuniv.edu.iq

[30] S. Mrabet, N. Ihzaz, M. N. Bessadok, C. Vázquez-Vázquez, M. Alshammari, and L. E. Mir, "Microstructural, raman, and magnetic investigations on CA-doped ZNO nanoparticles," Journal of Inorganic and Organometallic Polymers and Materials, vol. 34, no. 5, pp. 2064–2073, Dec. 2023, doi: 10.1007/s10904-023-02947-8.

[31] M. H. Gonfa and A. L. Birhanu, "Green synthesis, characterization and antibacterial evaluation of ZnO and Ag-doped ZnO nanoparticles using Ruta chalepensis leaf extract," Green Chemistry Letters and Reviews, vol. 17, no. 1, Oct. 2024, doi: 10.1080/17518253.2024.2412613.

[32] H. M. Rasheed, K. Aroosh, D. Meng, X. Ruan, M. Akhter, and X. Cui, "A Review on Modified ZnO to Address Environmental Challenges through Photocatalysis: Photodegradation of Organic Pollutants," Materials Today Energy, p. 101774, Dec. 2024, doi: 10.1016/j.mtener.2024.101774.

[33] M. I. Sayyed, A. Kumar, and Y. Maghrbi, "Impact of ZnO on the physical, mechanical, optical, and gamma-ray shielding properties of B2O3-Bi2O3-Na2O-ZnO-CaO glasses.," Optical Materials, p. 116171, Sep. 2024, doi: 10.1016/j.optmat.2024.116171.

[34] P. R. Jubu et al., "Considerations about the determination of optical bandgap from diffuse reflectance spectroscopy using the tauc plot," Journal of Optics, Feb. 2024, doi: 10.1007/s12596-024-01741-0.

[35] Y. Li, J. Li, M. Li, J. Sun, X. Shang, and Y. Ma, "Biological mechanism of ZnO nanomaterials," Journal of Applied Toxicology, vol. 44, no. 1, pp. 107–117, Jul. 2023, doi: 10.1002/jat.4522.

[36] V. P. K. De Maria et al., "Advances in ZnO nanoparticles in building material: Antimicrobial and photocatalytic applications – Systematic literature review," Construction and Building Materials, vol. 417, p. 135337, Feb. 2024, doi: 10.1016/j.conbuildmat.2024.135337.

*Corresponding author
Aseel S. Jasim,
Biomass Energy Department, Al-Nahrain Renewable Energy Research Center, Al-Nahrain University, Jadriya, Baghdad, Iraq
e-mail: aseelsubhi11@nahrainuniv.edu.iq